Shahrood University of Technology
Iranian Society of Mining Engineering (IRSME)
Journal of Mining and Environment (JME)
journal homepage: www.jme.shahroodut.ac.ir
THOMSON REUTERS

Vol. 11, No. 2, 2020, 467-480.
DOI: 10.22044/jme.2020.8710.1757

A 3D Discrete Element Analysis of Failure Mechanism of Shallow Foundations in Rocks

S. Sepehri, R. Shirinabadi*, N. Hoseini Alae, E. Moosavi and A.H. Bangian Tabrizi

Department of petroleum and Mining Engineering, South Tehran Branch, Islamic Azad University, Tehran, Iran

Received 19 July 2019; received in revised form 20 February 2020; accepted 21 February 2020

Keywords

Bearing capacity

Rock foundations

Shear failure mechanism

Particle flow code

Abstract

In this research work, a 3D numerical modeling technique is proposed based on the 3D particle flow code in order to investigate the failure mechanism of rock foundations. Two series of footings with different geometries and areas are considered in this work. The failure mechanism obtained is similar to that of the Terzaghi's but there is a negligible difference in between. Lastly, one equation is presented to calculate the bearing capacity based on the results achieved from the numerical model and the Mohr-Coulomb theory. The sensitivity analyses are performed on the friction angle, cohesion, and footing width. The results obtained are compared with the corresponding results given by the equations given by Terzaghi and Meyerhof. This comparison demonstrates a good agreement between them. In the friction angle sensitive analysis, the amounts of the bearing capacity diagram are very close to Meyerhof's, which overlap with each other.

Nomenclature

B	Width of footing
T	Length of footing
α	Internal angle between the failure under the footing with the horizontal direction
γ	Effective unit weight of foundation
C	Cohesion of foundation
$\emptyset$	Friction angel of foundation
I	Half width of footing
J	Maximum distance of the shear failure to the edge of the footing
l	Maximum distance between the outer edge of the shear failure surface and underlying edge of the Rankin active area
BC, CE, ED	Simplified failure surfaces
AC, AE, AB, AD, FB, FD	Auxiliary surfaces
DG	Height of the triangular Rankin active
A_1, A_2, A_3,	Shear failure surface areas (on the horizontal section)
A_4, A_5, A_6	Failure surface areas (on the vertical section)
Q', Q'', Q'''	Split of footing force on the failure surfaces
F_n	Normal force
$\sigma_{n1}, \sigma_{n2}, \sigma_{n3}$	Normal stresses
τ', τ'', τ'''	Shear stresses of failure surfaces
τ_1, τ_2, τ_3	Shear resistances of failure surfaces
Q	Force of footing
q_u	Ultimate bearing capacity
N_c, N_q, N_γ	Bearing capacity factors
$\lambda_{cd}, \lambda_{qd,} \lambda_{\gamma d}$	Depth factors
$\lambda_{ci}, \lambda_{qi}, \lambda_{\gamma i}$	Load inclination factors
$\lambda_{cs}, \lambda_{qs}, \lambda_{\gamma s}$	Shape factors

1. Introduction

In the analysis of the foundation, one of the important issues is to deliberate the bearing capacity. This matter is considered as a substantial part of geotechnical engineering operations [1]. Prandtl (1921) was the one who first scrutinized the penetration of a rigid body into a soft body. Afterward, Reissner (1924) introduced the bearing capacity theory based on the concept of plastic stability. Later, the formulations were reformed by Terzaghi (1943), Meyerhof (1963), Hansen (1969), Vesic (1975), and others [2]. In 1943, Terzaghi was

Corresponding author: R_Shirinabadi@azad.ac.ir (R. Shirinabadi).

the first to present a theory for evaluating the ultimate bearing capacity of a strip footing on rigid shallow foundations. He used the semi-empirical equation and indicated that the internal angle of the Rankin active area was equal to (∅). After that, in 1963, Meyerhof proposed various correction factors and modified the equations for the bearing capacity. The bearing capacity of a shallow foundation is commonly determined using the Terzaghi's classical bearing capacity equation [22]. Table 1 shows the basic and primary equations of bearing capacity [3, 20]. Footing and foundation are shown in Figure 1.

Figure 1. Footing and foundation.

Table 1. Basic and primary equations of bearing capacity [3, 20].

Terzaghi (1943)	$q_u = \frac{Q}{BT} = cN_c + qN_q + \frac{1}{2}\gamma BN_\gamma$
Meyerhof (1963)	$q_u = \frac{Q}{BT} = c\lambda_{cs}\lambda_{cd}\lambda_{ci}N_c + q\lambda_{qs}\lambda_{qd}\lambda_{qi}N_q + \frac{1}{2}\gamma B\lambda_{\gamma s}\lambda_{\gamma d}\lambda_{\gamma i}N_\gamma$

Since there are difficulties in obtaining the bearing capacity in the laboratory and on-site, the researchers have been trying to explore simpler methods estimating the bearing capacity [5]. The classical formulations are subject to restrictions and assumptions, and they do not always provide reasonable results when compared to the available experimental data [6]. Within the last few decades, numerical methods and models have been remarkably developed in rock mechanics [7]. Some of these models include the finite difference method, finite element method, distinct element method, and boundary element method. There are also several models of materials in the related software simplifying the analysis applied by the researchers to investigate the behavior of rocks [8, 9]. It is promising to discover the interactions among diverse factors with the advent of sensitivity analysis methods even though, some numerical models are not able to completely clarify the problem [10, 11]. Many researchers have developed different methods to evaluate the bearing capacity in order to avoid the onsite techniques. Notwithstanding this fact, it is inevitable to develop more influential predictive models [2].

Although the researchers have carried out various investigations on soil foundation, the influences of failure mechanism of rock foundation and the effect of the footing geometry and its area have not been remarkably studied yet. For example, Fernando (2011) has proved that the footing geometry impact the bearing capacity, which has a higher value in conic and pyramidal footings than in flat ones in a dry sand experiment [12]. Dixit (2013) has practiced the rectangular footing placed on sand in the laboratory and demonstrated that the trend of the ultimate bearing capacity is proliferated through increasing the footing area [5]. In 2014, Ramandan has used the physical experiment and numerical model and has indicated that scaling up the footing area results in increasing the bearing capacity of the foundation [13]. Castelli (2015) has used the square and strip footings placed on the sand to do a series of experiments. As a result, he could indicate that the enhancement of footing dimensions increased the bearing capacity [14]. In 2017, Acharyya has used the FLAC software and has ascertained that the bearing capacity rises through scaling up the width of footing [15].

2. Discrete element method

The particle flow code was used in the PFC3D software, version 5.00.27, so as to make the numerical model. The particle flow code in three dimensions (PFC3D) is a commercial software package based on the discrete element method [16, 17]. PFC is an advanced, fast, and particularly versatile commercial, multi-physics simulation software for engineers and scientists applying the Distinct Element Method (DEM). As PFC is highly efficient and precise, it has improved sciences related to earth sciences, mining, rock mechanics, and geotechnics. The stepping algorithm of this study is shown in Figure 2

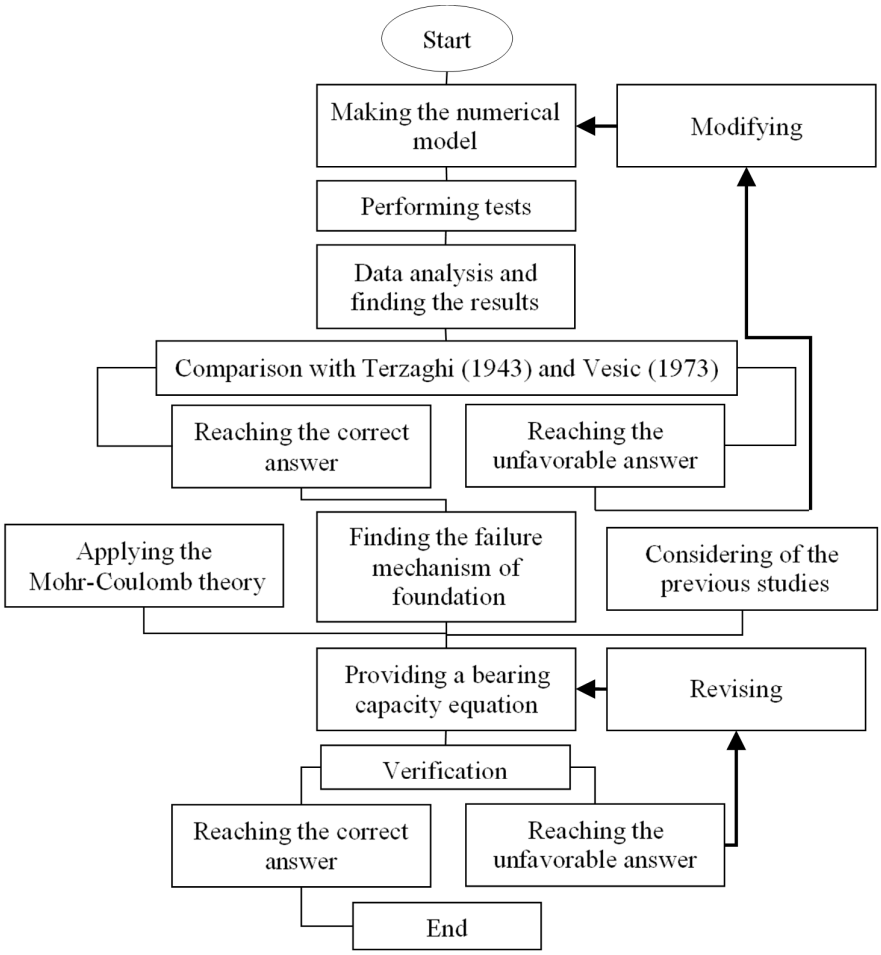

Figure 2. Stepping algorithm to make the numerical model and obtain the ultimate bearing capacity.

2.1. Materials and properties

The grains used for foundation modeling were in dimensions of 4.75-12.5 mm, which were similar to the fine gravel of Jalilabad zone in the east of Tehran (Iran). To numerically mimic a relatively rock-like material, it is required to stick these granular particles through a bonded model [18]. The behavioral model used in PFC3D was the parallel bond model. The mechanical properties were considered the same as the granite for the foundation, and all numerical experiments were performed on a rock foundation. The grain-size distribution diagram obtained from PFC3D is depicted in Figure 3. The mechanical properties given to the foundation in the numerical model are similar to those in Table 2.

2.2. Establishment of model geometry

In this work, the sample box was in sizes of 700 mm (L), 400 mm (H), and 400 mm (D) filled by grains up to the height of 350 mm. Figure 4 illustrates the numerical model. Two series of footings were employed with a fixed area but in square, rectangular, and circular geometries. Table 3 displays the dimensions and geometries of the footings.

Table 2. Mechanical properties of the foundation.

Row	Parameters	Unit	Value
1	Uniaxial compressive strength	MPa	99
2	Cohesion	MPa	16.5
3	Angle of friction	Deg.	50
5	Density	Kg/m^3	2460

Table 3. Dimension and geometry of the numerical model footings.

No.	Area (cm^2)	Geometry	Dimension (cm)
1	64	Square	8×8
2	64	Rectangle	7×9, 14
3	64	Circle	4.51 R
4	49	Square	7×7
5	49	Rectangle	6×8, 16
6	49	Circle	3.95R

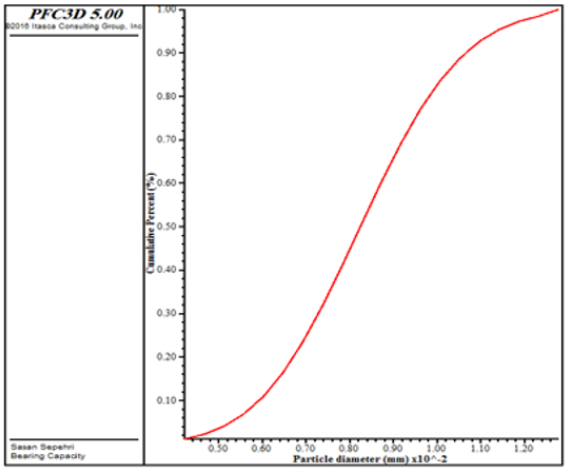

Figure 3. Grain-size distribution diagram of PFC3D.

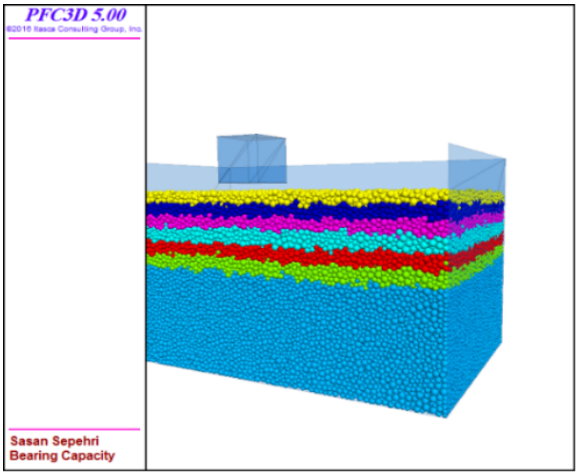

Figure 4. 3D numerical model of the rock foundation.

3. Results and discussion

3.1. Investigation of footing effect

Figure 5 reveals the displacement–force diagram for the square footing with the area of 64 cm^2. A general shear failure is made in the foundation. At this point, the displacement-force diagram totally reverted, which was coped within the outlook of Vesic in 1973 [19]. After several experiments were observed and the diagrams were monitored, it was determined that the displacement-force diagram included three parts before the failure point. Figure 5 indicates that section A is related to the closure of unfilled spaces inside the foundation. In part A, the footing movement will be faced with foundation resistance because the Rankin active area is not formed under the footing. Hence, the slope of the diagram is low in the displacement-force diagram in Section A. The Rankin active area is shaped with a semi-circular tip and the slope of the graph increases in section B, and at this point, the uplift starts close to the footing. Eventually, the Rankin active area is completely made in part C of the displacement-force diagram. This occurs when the grains are separated from their places and are located in a manner that the Rankin active area is completely formed. In part C, the highest penetration rate of the footing into the foundation is observed. The displacement-force diagram of the foundation is featured out in Figure 5.

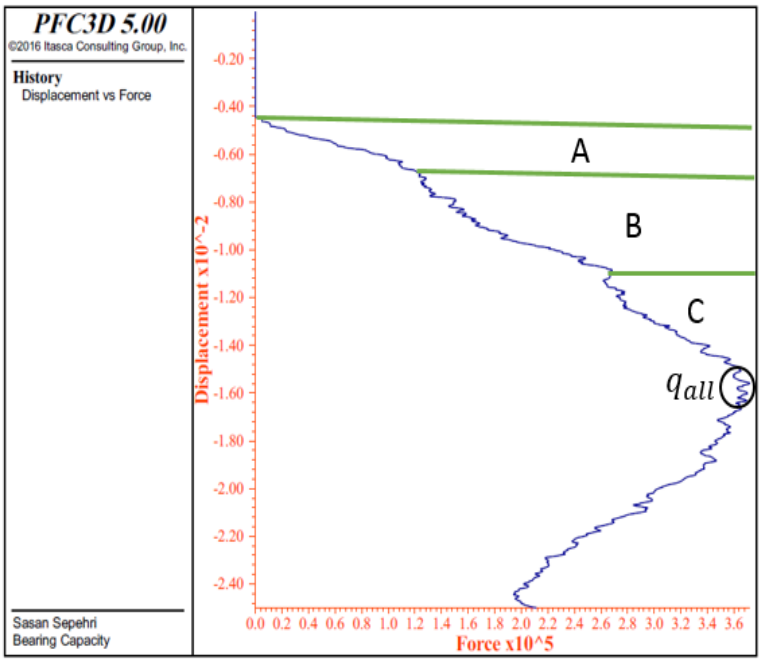

Figure 5. Displacement - force diagram for a square footing of 68 cm^2 area.

After the test was done, it was concluded that the bearing capacity for a circular footing would be more than that of the others. Furthermore, the bearing capacity of a rectangular footing is less than that of a square. Table 4 shows the results taken from the numerical experiments.

Table 4. Numerical test results.

No.	Geometry	Area (cm^2)	Dimension (cm)	Force (KN)	Settlement (cm)
1	Square	64	8×8	370	1.12
2	Rectangle	64	7×9, 14	350	1.14
3	Circle	64	4.51 R	400	1.13
4	Square	49	7×7	272	0.93
5	Rectangle	49	6×8.16	264	1.02
6	Circle	49	3.95 R	320	0.99

Previously, the researchers indicated that scaling up of the footing area resulted in increasing the bearing capacity. In this research work, the particle flow modeling proved this issue for all three square, rectangular, and circular footings in rock foundation. Also it was determined that the circular, square, and rectangular footings had scored the highest bearing capacity, correspondingly. Furthermore, it was specified that increasing the footing area enhanced the bearing capacity and settlement but changing the footing geometry did not considerably affect the settlement. Thus there are two mechanisms, one is related to the footing area where the bearing capacity and settlement will be changed, and the other one is related to the footing geometry where the bearing capacity is only changed.

3.2. Failure mechanism of rock foundation

In this research work, it was demonstrated that the Rankin active area was the triangle in two dimensions and the wedge in three dimensions. If the foundation is made up of heterogeneous grain-size distribution, the internal angles of the two sides of the Rankin active area are different. Indeed, the Rankin active is formed in an asymmetric pattern.

The present work confirmed and evidenced the influence of grain-size distribution on the shape of the Rankin active area. Figure 6 indicates that this area is formed in an asymmetric triangle in a 2D cross-section. The tilt in the structure results in an asymmetrical distribution of force under the footing where an asymmetric tringle has been made. Many structures have experienced tilting. Thus it is demonstrated that the heterogeneity of the grain-size distribution of the foundation should be considered as one of the most essential factors.

If the displacement-force diagram crosses out part A (Figure 4), elastic deformation finishes, plastic deformation begins in the foundation, and the wedge (Rankin active area) starts to form. Consequently, if the grain-size distribution is not homogeneous in the foundation, an asymmetric wedge is automatically formed. Eventually, the exiting force from the center of the footing and a torque force make the structure tilt to one side. Figure 6 displays a Rankin active area that can be observed as an asymmetric triangle. In this asymmetric triangle, one of the internal angles is less than (∅) and the other angle is more than (∅). Nonetheless, the angles are close to (∅). It is concluded that the internal angles of the triangle Rankin active area in the rock foundation are equal to (∅) if the influence of the heterogeneity of the grain-size distribution is ignored.

An asymmetric uplift is made around the footing for the sake of the presence of asymmetric Rankin active area. Furthermore, the failure shape in the area of radial shear and the area of Rankin passive will be different on each side of the footing. As observed in Figure 7, the highest displacements of the grains are blue-colored and are positioned on the left side of the footing. Consequently, as indicated in Figure 8, the highest displacements of the grains are yellow-colored and are positioned on the left side of the footing. According to these findings, it is demonstrated that the highest displacement of the grains has occurred on the left side of the footing.

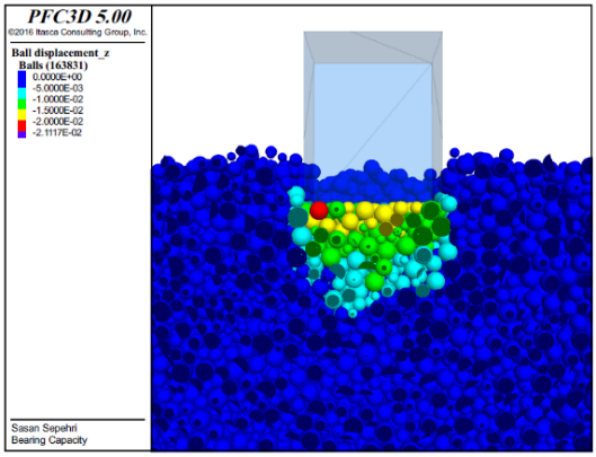

Figure 6. Failure triangle under the footing with 8 * 8 cm dimension (Rankin active area).

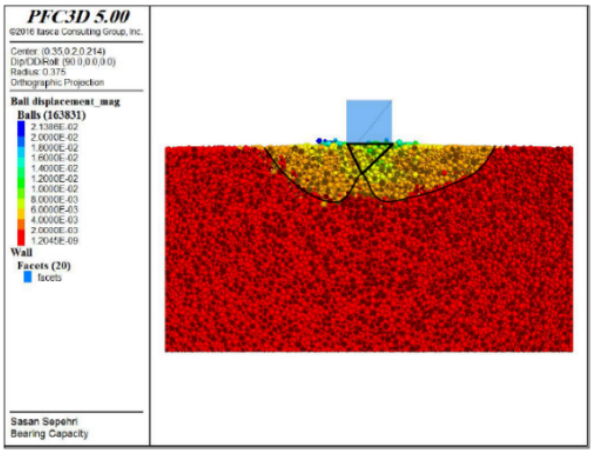

Figure 7. General shear failure of the rock foundation.

When the footing is penetrated more into the foundation, a symmetric triangle is formed under the footing, and consequently, the area of radial shear and Rankin passive area will also be symmetrical. According to our knowledge from this numerical model, the cube box with descending fixed movement was applied as the footing, and the symmetric triangle was made by the separated and displaced grains. The general shear failure is developed like that of Terzaghi's (Figure 7).

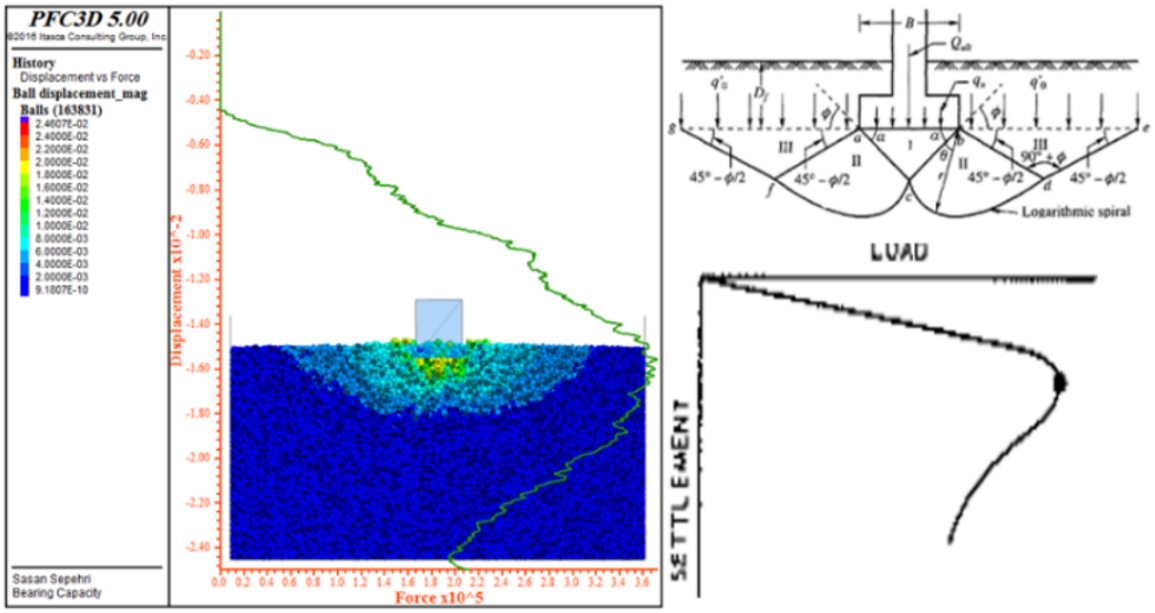

Figure 8. Particle flow model of the general shear failure of the rock foundation (compared with Terzaghi (1943)'s failure mechanism and Vesic (1973)'s bearing capacity diagram).

Figure 9 exhibits the displacements that have been filtered in both the positive and negative directions of the X-axis (the length of the test box). In consequence, two zones (one on the right side and the other on the left side of the footing) will be developed. It should be pointed out that these zones are similar to the radial shear zone in the Terzaghi's (1943) failure mechanism.

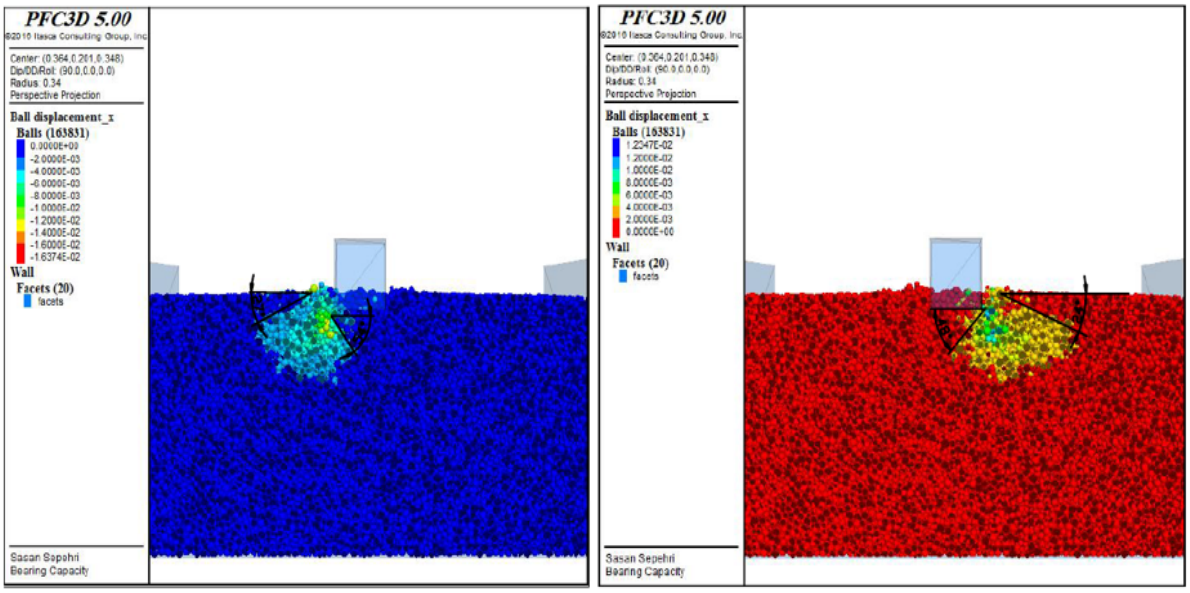

Figure 9. Grains with positive and negative horizontal displacement in the rock foundation.

Figure 10 discloses the displacements that have been filtered in the positive direction of the Z-axis. Clearly, it is in the direction of the test box height. As a result, two areas will be made (one on the right side and the other on the left side of the footing). The areas are like the Rankin passive area in the Terzaghi's (1943) failure mechanism.

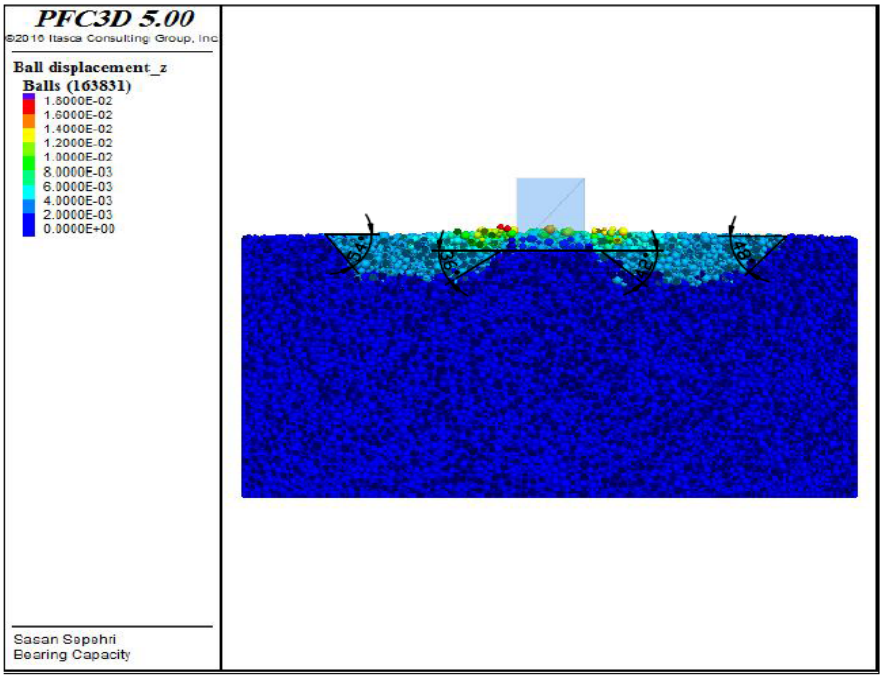

Figure 10. Grains with an ascending motion in the rock foundation.

These images were put on one another so that the failure mechanism would be specified. Figure 11 implies that there will be commonly four areas for each side of the foundation. In part A, the grains are moved downward. In part B, the grains are moved almost horizontally. In part C, the grains are moved almost vertically; thus, they bring about the uplift phenomenon. At the area shared by parts B and C, there is an area known as part D in which the grains are moved to the horizontal and vertical sides.

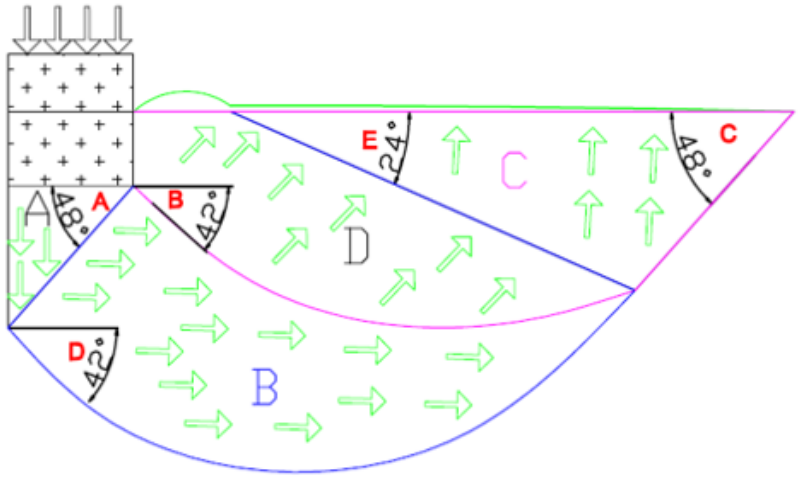

Figure 11. Shape of the general shear failure mechanism in the rock foundation (parts B and C are shown in blue and purple boundaries, respectively).

3.3. Equation of bearing capacity

The failure mechanism in Figure 12 and the Mohr-Coulomb failure criterion contributed to make a formulation to calculate the bearing capacity. Figure 12 shows all of the factors that are used in the formulation.

According to Figure12 and Appendix A, since the failure surface of EC is a considerably larger area than the other failure surfaces, it will be able to play a leading role in general shear failure and bearing capacity. Thus when the shear stress of EC surface (τ_2) is greater than the resistance of EC surface (τ''), the general shear failure emerges as follows:

$$(\sigma_{n2} tan\emptyset + C) = Q''/A_5 \quad (1)$$

$$(\sigma_{n2} tan\emptyset + C) = \frac{Q.cos\,\alpha\,.sin\,{}^{\alpha}/_{2}}{A_5} \quad (2)$$

$$Q.cos\,\alpha\,.sin\,{}^{\alpha}/_{2} = (A_5.\sigma_{n2} tan\emptyset + A_5.C) \quad (3)$$

$$Q = \frac{(A_5.\sigma_{n2}.tan\emptyset + A_5.C)}{cos\,\alpha\,.sin\,{}^{\alpha}/_{2}} \quad (KN) \quad (4)$$

Since one side of the footing is considered, the amount of (Q) is multiplied by 2. Eventually, the bearing capacity of the foundation will be calculated by the following equation:

$$q_u = \frac{2Q}{B.T} \quad (\frac{KN}{m^2}) \quad (5)$$

The amount of (q_u) includes the bearing capacity of the foundation for one footing in the dimensions of (B $*$ T). The mechanical properties of the foundation are equal to $\emptyset = c_1{}^{\circ}$, $C = c_2 \frac{KN}{m^2}$, and $\gamma = c_3 \frac{KN}{m^3}$.

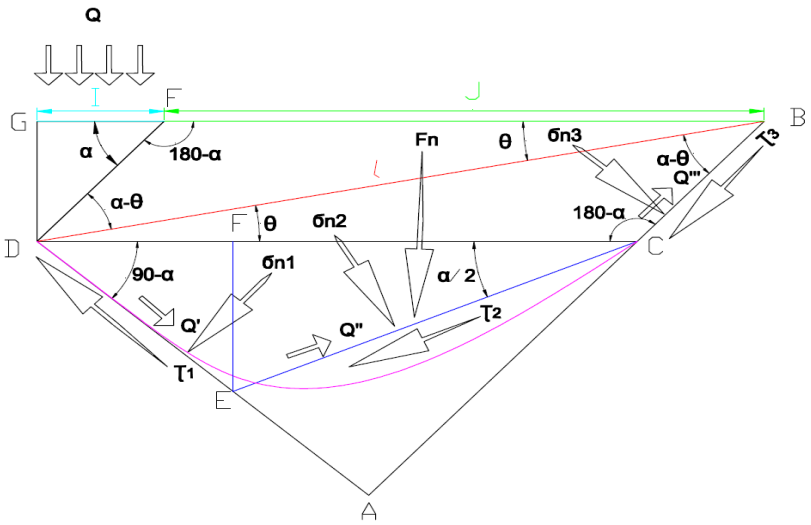

Figure 12. Bearing capacity formulation factors that show on simplified failure mechanism shape.

3.3.1. Verification of equation

The sensitivity analysis was performed on the friction angle, cohesion, and footing width. The obtained results of the new equation were compared with the Terzaghi and Meyerhof's equation results. The results were close together.

3.3.1.1. Sensitivity analysis of friction angle

In the sensitivity analysis of the friction angle, the amounts of (C = 9.8 $\frac{KN}{m^2}$) and (γ = 17.6 $\frac{KN}{m^3}$) were considered to be constant. The bearing capacity amounts for the 10, 20, 30, 40, and 50 degrees of the friction angle were obtained. For this work, one footing in dimensions of 4 * 4 m was considered. The results were illustrated in the graph of Figure 13.

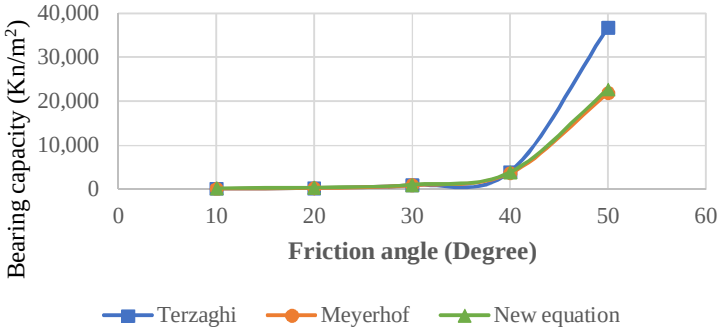

Figure 13. Sensitivity analysis of the friction angle.

According to Figure 13, the bearing capacity resulting from the new equation was similar to the Meyerhof and Terzaghi's equation, in the friction angle sensitivity analysis. Definitely, the amounts were growing in the same ratio and they were very close to the Meyerhof. The two graphs overlapped each other. All three equations were divulging a higher growth rate in a high friction angle.

3.3.1.2. Sensitivity analysis of cohesion

In the sensitivity analysis of the cohesion, the amounts of ($\emptyset$ = 20°) and (γ = 17.6 $\frac{KN}{m^3}$) were considered to be constant. The bearing capacity amounts for the 10, 20, 30, 40, and 50 $\frac{KN}{m^2}$ of cohesions were obtained. For this purpose, one footing in dimensions of 4 × 4 m was used. Figure 14 shows the results.

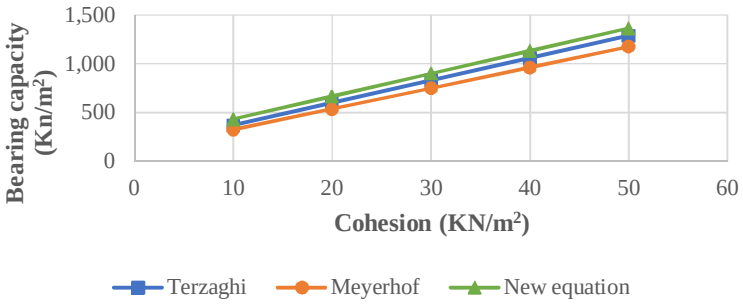

Figure 14. Sensitivity analysis of the cohesion.

Based on Figure 14, it was clear that the bearing capacity obtained from the new equation obeys the similar mechanism of Terzaghi and Meyerhof in the cohesion sensitivity analysis. Also the amounts were growing the same, and they were close to Terzaghi and Meyerhof.

3.3.1.3. Sensitivity analysis of footing width

In the sensitivity analysis of the footing width, the amounts of (C = 9.8 $\frac{KN}{m^2}$), (γ = 17.6 $\frac{KN}{m^3}$), and ($\emptyset$ = 20°) are supposed to be constant. The amounts of the bearing capacity were calculated from the width of footing for the amounts of 1, 2, 3, 4, and 5 m. The graph of Figure 15 features the results.

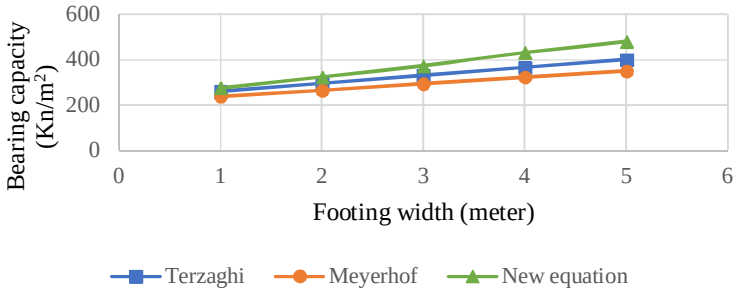

Figure 15. Sensitivity analysis of the footing width.

As shown in Figure 15, it is evident that the bearing capacity obtained from the new equation obeys the similar mechanism of Terzaghi and Meyerhof in the sensitivity analysis of the footing dimensions. The amounts were growing the same. However, the amounts of Terzaghi and Meyerhof are more conservative.

4. Conclusions

A 3D numerical modeling approach was used based on the 3D particle flow code (PFC3D). The failure mechanism in this work and the Mohr-Coulomb failure criterion contributed to make the equation to calculate the bearing capacity.

Eventually, the following conclusions may be gained from the results of this research work:

- According to Figure 4, the end of region B is considered as the critical point. The reason is that the active Rankin triangle is completely formed under the footing in region C. Thus an asymmetric triangle is automatically formed because the grain-size distribution is not homogeneous in the foundation. After this asymmetric triangle is made, the forced exit from the footing center and soil tends to exit more from one side of the footing. This causes the subsidence and tilting of the structure.
- According to the results obtained from the numerical model based on the 3D particle flow theory, the circular footings have a higher bearing capacity than the square and rectangular footings.
- According to Figure 11, the particles horizontally move in region B. The particles vertically move in region C. The particles move in an aslant pattern (horizontal and vertical) in region D. This subject is very important in improvement. Clearly, considering the drilling angles leads to better results in ground improvement (anchoring, nailing, and piling methods) based on the movement of the particles in the three aforementioned regions.
- As the new formula is proved in a way different from the formulas of Terzaghi and Meyerhof, Figures. 13 to 15 indicate that the development pattern of the graphs follows the same patterns. The only difference is that the amounts of bearing capacity in the new formula is somehow higher than the formulas of Terzaghi and Meyerhof. This subjects to economize the construction cost of the foundation.

References

[1]. Baazouzi, M. (2016). 2D Numerical Analysis of Shallow Foundation Rested Near Slope under Inclined Loading. Elsevier. Procedia Engineering, 143: 623-634. https://doi.org/10.1016/j.proeng.2016.06.086.

[2]. Tajeri, Sh. (2015). Indirect estimation of the ultimate bearing capacity of shallow foundations resting on rock masses. International Journal of Rock Mechanics & Mining Sciences, Elsevier Ltd. 107–117. https://doi.org/10.1016/j.ijrmms.2015.09.015.

[3]. Terzaghi K. (1943). Theoretical Soil Mechanics.

[4] Meyerhof, G.G. (1963). Some recent research on the bearing capacity of foundations. Can. Geotech. 1 (1): 16-26.

[5]. Dixit, M.S. (2013). Experimental Estimate of Ultimate Bearing Capacity and Settlement for Rectangular Footings. International Journal of Civil Engineering and Technology (IJCIET), 4 (2).

[6]. Tahmasebi poor, A., Barari, A., Behnia, M. and Najafi, T. (2015). Determination of the ultimate limit states of shallow foundations using gene expression programming (GEP) approach. Soils and Foundations, 55(3): 650-659. https://doi.org/10.1016/j.sandf.2015.04.015.

[7]. Israelsson, J.I. (1996). Short Descriptions of UDEC and 3DEC. In O. Stephansson, L. Jing, & C.-F. Tsang

(Eds.), Developments in Geotechnical Engineering, 79: 523-528.

[8]. Bretas, E.M., Léger, P. and Lemos, J.V. (2012). 3D stability analysis of gravity dams on sloped rock foundations using the limit equilibrium method. Computers and Geotechnics, 44.

[9]. Lin, Y., Zhu, D., Deng, Q. and He, Q. (2012). Collapse Analysis of Jointed Rock Slope Based on UDEC Software and Practical Seismic Load. Procedia Engineering, 31: 441-446. https://doi.org/10.1016/j.proeng.2012.01.1049.

[10]. Souley, M. and Homand, F. (1996). Stability of jointed rock masses evaluated by UDEC with an extended Saeb-Amadei constitutive law. International Journal of Rock Mechanics and Mining Sciences & Geomechanics Abstracts, 33(3): 233-244. https://doi.org/10.1016/0148-9062 (95)00063-1.

[11]. Zhou, H.-z., Zheng, G., Yu, X.-x., Zhang, T.-q. and Liu, J.-j. (2018). Bearing capacity and failure mechanism of ground improved by deep mixed columns. Journal of Zhejiang University-SCIENCE A, 19(4): 266-276. https://doi.org/10.1631/jzus.A1700517.

[12]. Fernando, N., Sendanayake, E., Sendanayake, D. and and Silva, N.D. (2011). The Experimental Investigation of Failure Mechanism and Bearing Capacity of Different Types of Shallow Foundation. Civil Engineering Research for Industry, Department of Civil Engineering, University of Moratuwa.

[13]. Ramadan, M.I. and Hussien, M.H. (2015). Bearing Capacity of Sand Overlying Clay – Strip Footing. International Journal of Science and Research (IJSR). 4 (11).

[14] Castelli, F., Lentini, V. and Dean, E.T. (2015). Evaluation of the Bearing Capacity of Footings on Slopes. International Journal of Physical Modelling in Geotechnics, 15 (3): 165-168.

[15]. Acharyya, R. and Dey, A. (2017). Finite Element Investigation of the Bearing Capacity of Square Footings Resting on Sloping Ground. INAE Letters, 2 (3): 97-105. https://doi.org/10.1007/s41403-017-0028-6

[16]. Potyondy, D.O. and Cundall, P.A. (2004). A bonded-particle model for rock. Int. J. Rock Mech. Min. Sci. 41: 1329–1364.

[17]. Itasca Consulting Group Inc. (2008). PFC3D-Particle Flow Code in Three Dimensions, version 4.0; Itasca Consulting.

[18]. Mas Ivars, D.M., Pierce, M.E., Darcel, C., Juan, R.M., Potyondy, D.O., Young, R.P. and Cundall, P.A. (2011). The synthetic rock mass approach for jointed rock mass modelling. Int. J. Rock Mech. Min. Sci. 48: 219–244.

[19]. Vesic, A.S. (1973). Analysis of Ultimate Loads of Shallow Foundations. Journal of the Soil Mechanics and Foundations Division, 99 (1): 45-73. https://doi.org/10.1016/0148-9062(74)90598-1.

[20]. Das, B.M. (2010). Principles of Foundation Engineering. 7th Ed, International Edition, 143-145.

[21]. Meyerhof, G.G. (1963). Bearing Capacity of Concrete and Rock. Magazine of Concrete, April. https://doi.org/10.1680/macr.1953.4.12.107.

[22]. Chavda, J.T. and Dodagoudar, G.R. (2019). Finite Element Evaluation of Vertical Bearing Capacity Factors N'_c, N'_q and N'_γ for Ring Footings, Geotech Geol Eng, 37, 741–754, https://doi.org/10.1007/s10706-018-0645-1.

[23]. Qiang, C. (2018). The efects of the geometric parameters of a circular shallow foundation on its uplift bearing capacity in loess soil. Acta Geotechnica Slovenica, 2: 74-80. https://doi.org/10.18690/actageotechslov.15.2.

[24]. Chen, Q. (2015). Ultimate bearing capacity analysis of strip footings on reinforced soil foundation. Elsevier, Soils and Foundations Journal, 55(1): 74–85. https://doi.org/10.1016/j.sandf.2014.12.006.

[25]. Latha, G.M. and Somwanshi, A. (2009). Effect of reinforcement form on the bearing capacity of square footings on sand, Elsevier, Geotextiles and Geomembranes, 27:409–422.

[26]. Bowels, J.E. (1997). Foundation analysis and design. Fifth edition.

Appendix A

According to Figure 12, in the radial shear zone and the passive Rankin zone, the grain-size distribution is effective. That is why it is difficult to identify these zones in reality. Indeed, DE, EC, and BC can be practiced as a replacement for the radial shear and the passive Rankin zones. Figure 16 shows the 3D shapes of failure surfaces in general failure mechanisms of bearing capacity.

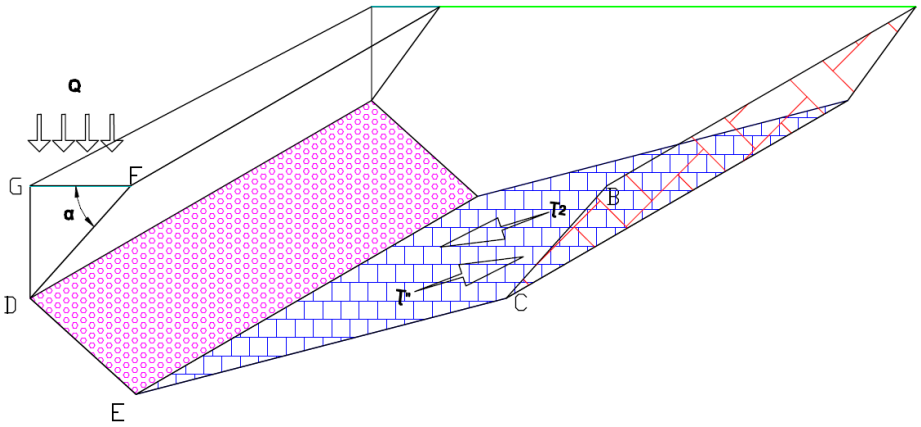

Figure A1. 3D shape of failure surfaces (A4 surface is purple, A5 surface is blue, A6 surface is red).

For a foundation with width B:

$$I = \frac{B}{2} \quad \text{(A-1)}$$

The (J) and (α) values can be experimentally figured out by the dimension of the footing, friction angle, cohesion, and density. The ε, δ, ω, ∂, ε', δ', ω', ∂' parameters are considered constant amounts in the following:

$$J = \varepsilon x + \delta \emptyset + \omega C + \partial \gamma \quad \text{(A-2)}$$

$$\alpha = \varepsilon' x + \delta' \emptyset + \omega' C + \partial' \gamma \approx \emptyset \quad \text{(A-3)}$$

The following equations can be used to calculate (y) (Terzaghi 1943):

$$J = 2r\, e^{\beta \tan \emptyset} \cos(45 - \frac{\emptyset}{2}) \quad \text{(A-4)}$$

$$\beta = 135 - \frac{\emptyset}{2} \rightarrow \frac{\pi}{180} \quad \text{(A-5)}$$

$$r = \frac{x}{\cos \emptyset} \quad \text{(A-6)}$$

Based on the available values, the values for (l) and (θ) can be obtained:

$$l^2 = J^2 + \frac{I^2}{\cos^2 \alpha} - \frac{2IJ}{\cos \alpha} . \cos(180 - \alpha) \rightarrow \quad \text{(A-7)}$$

$$\rightarrow l^2 = J^2 + \frac{x^2}{\cos^2 \alpha} + 2IJ \rightarrow \quad \text{(A-8)}$$

$$\rightarrow l = \sqrt{J^2 + \frac{I^2}{\cos^2 \alpha} + 2IJ} \quad \text{(A-9)}$$

$$\frac{l}{\sin \alpha} = \frac{I/\cos \alpha}{\sin \theta / 1} \rightarrow \quad \text{(A-10)}$$

$$\rightarrow \sin \theta = \frac{I . \sin \alpha}{l . \cos \alpha} = \frac{I}{l} tg\alpha \rightarrow \quad \text{(A-11)}$$

$$\rightarrow \theta = \sin^{-1}(\frac{I}{l} tg\alpha) \quad \text{(A-12)}$$

$$AB = l . \sin(90 - \alpha + \theta) \rightarrow \quad \text{(A-13)}$$

$$\rightarrow AB = l . \cos(\alpha - \theta) \quad \text{(A-14)}$$

$$AD = l . \cos(90 - \alpha + \theta) \rightarrow \quad \text{(A-15)}$$

$$\rightarrow AD = l . \sin(\alpha - \theta) \quad \text{(A-16)}$$

$$BC = \frac{I}{\cos \alpha} \quad \text{(A-17)}$$

$$AC = AB - BC \quad \text{(A-18)}$$

$$AE = AC . \tan \alpha/2 \quad \text{(A-19)}$$

$$DE = AD - AE \quad \text{(A-20)}$$

$$EC = \frac{AC}{\cos \alpha/2} \quad \text{(A-21)}$$

$$FD = DE . \cos(90 - \alpha) \quad \text{(A-22)}$$

$$FC = EC . \cos \alpha/2 \quad \text{(A-23)}$$

$$EF = DE . \cos \alpha \quad \text{(A-24)}$$

$$DG = I . \tan \alpha \quad \text{(A-25)}$$

$$A_1 = \frac{1}{2} . EF . FD \quad \text{(A-26)}$$

$$A_2 = \frac{1}{2} . EF . FC \quad \text{(A-27)}$$

$$A_3 = DG.J \quad \text{(A-28)}$$

$$A_4 = DE.T \quad \text{(A-29)}$$

$$A_5 = EC.T \quad \text{(A-30)}$$

$$A_6 = BC.T \quad \text{(A-31)}$$

$$Q' = Q.\cos\alpha \quad \text{(A-32)}$$

$$Q'' = Q'.\sin{}^{\alpha}/_{2} \quad \text{(A-33)}$$

$$Q''' = Q''.\cos{}^{\alpha}/_{2} \quad \text{(A-34)}$$

Initially, all the effective parameters in the failure mechanism are obtained (Figure 12). After that, the bearing capacity is calculated with the contribution of the Mohr-Coulomb equation.

If (T) is equal to the second side of the footing, the force obtained from the overburden is equal to:

$$F_n = (A_1 + A_2 + A_3).T.\gamma \quad \text{(A-35)}$$

Normal stresses made by overburden force are equal to:

$$\sigma_{n1} = \frac{F_n}{A_4}.\sin\alpha \quad \text{(A-36)}$$

$$\sigma_{n2} = \frac{F_n}{A_5}.\cos{}^{\alpha}/_{2} \quad \text{(A-37)}$$

$$\sigma_{n3} = \frac{F_n}{A_6}.\sin\theta \quad \text{(A-38)}$$

$$\tau_1 = (\sigma_{n1}\tan\emptyset + C) \quad \text{(A-39)}$$

$$\tau_2 = (\sigma_{n2}\tan\emptyset + C) \quad \text{(A-40)}$$

$$\tau_3 = (\sigma_{n3}\tan\emptyset + C) \quad \text{(A-41)}$$

The shear stresses caused by force (q) are equal to:

$$\tau' = Q'/A_4 \quad \text{(A-42)}$$

$$\tau'' = Q''/A_5 \quad \text{(A-43)}$$

$$\tau''' = Q'''/A_6 \quad \text{(A-44)}$$

$$(\sigma_{n2}\tan\emptyset + C) = Q''/A_5 \quad \text{(A-45)}$$

$$(\sigma_{n2}\tan\emptyset + C) = \frac{Q.\cos\alpha.\sin{}^{\alpha}/_{2}}{A_5} \quad \text{(A-46)}$$

$$Q.\cos\alpha.\sin{}^{\alpha}/_{2} = (A_5.\sigma_{n2}\tan\emptyset + A_5.C) \quad \text{(A-47)}$$

$$Q = \frac{(A_5.\sigma_{n2}.\tan\emptyset + A_5.C)}{\cos\alpha.\sin{}^{\alpha}/_{2}}(KN) \quad \text{(A-48)}$$

$$q_u = \frac{2Q}{B.T}\left(\frac{KN}{m^2}\right) \quad \text{(A-49)}$$

آنالیز مکانیزم گسیختگی با استفاده از المان مجزای سه بعدی برای پی‌های سطحی در سنگ

ساسان سپهری، رضا شیرین آبادی*، نوید حسینی علائی، احسان موسوی و امیرحسین بانگیان تبریزی

گروه مهندسی نفت و معدن، واحد تهران جنوب، دانشگاه آزاد اسلامی، تهران، ایران

ارسال 2020/1/13، پذیرش 2020/2/14

* نویسنده مسئول مکاتبات: r_shirinabadi@azad.ac.ir

چکیده:

در این تحقیق، یک مدل عددی بر مبنای تئوری جریان ذرات سه بعدی به منظور بررسی گسیختگی فونداسیون‌های سنگی استفاده شده است. دو سری پایه با هندسه و مساحت متفاوت بکار گرفته شده است. مکانیزم گسیختگی بدست آمده با وجود تفاوت های جزئی مشابه نظر ترزاقی است. با توجه به نتایج بدست آمده، یک فرمول به منظور محاسبه ظرفیت باربری ارائه شد. در این فرمول از تئوری شکست موهر – کولمب استفاده شده است. یک آنالیز حساسیت بر روی زاویه اصطکاک داخلی، چسبنگی و عرض پایه انجام گرفت. نتایج بدست آمده با روابط ترزاقی و مایرهوف مقایسه گردید. این مقایسه نمایشگر یک تطابق مناسب مابین نتایج بدست آمده است. برای مثال، در زاویه اصطکاک داخلی، مقادیر نمودار ظرفیت باربری بسیار نزدیک به رابطه مایرهوف بوده و نمودار آنها یک همپوشانی را نشان می‌دهد.

کلمات کلیدی: ظرفیت باربری، فونداسیون سنگی، مکانیزم گسیختگی برشی، کد جریان ذرات.